

GSA Data Repository Item DR2006160

Apatite (U-Th)/He signal of large magnitude and accelerated glacial erosion: southwest British Columbia

By: T.A. Ehlers, K.A. Farley, M.E. Rusmore, G.J. Woodsworth

Appendix A: Apatite (U-Th)/He Thermochronometer Data

Methods and Data

Apatites were separated using conventional heavy-liquid and magnetic separation techniques and sieved to 100-150 μm minimum dimension. Euhedral and inclusion-free grains were hand-picked under a 120x binocular microscope with cross polars, measured for α emission correction (Farley et al., 1996), loaded into Pt capsules, and out-gassed under a laser at 1100 °C for 5 minutes. Evolved helium was spiked with ^3He , cryogenically concentrated and purified, and the $^4\text{He}/^3\text{He}$ ratio measured on a quadrupole mass spectrometer. After out-gassing, the grains were retrieved, dissolved in HNO_3 , spiked with ^{235}U and ^{230}Th , and Th and U isotope ratios analyzed by ICPMS. The propagated analytical uncertainty on these He ages is $\sim 2\%$ 1σ (Farley, 2000).

Table 1 shows the apatite (U-Th)/He data used in this study. Figure DR1 shows the sample locations, ages, and ID numbers. The reported sample uncertainties were calculated in the following way:

(1) Twelve of our samples had replicate analyses. Of these samples, 5 had a 6% (2σ) uncertainty. Three samples had $< 6\%$ uncertainty, and 4 samples had $> 6\%$ uncertainty. The assigned 6% uncertainty for samples without replicate analyses was the average uncertainty from replicate analyses. If during an age determination any peculiarities were noted a replicate analysis was performed. Thus, the uncertainties calculated from samples with replicate analyses are the worst case scenario and the error derived from them for other samples is conservative.

(2) Furthermore, work by Farley et al. (2001) in the same plutonic complex and lithologies in the northern Coast Mountains found that replicate analyses from 29 out of 55 samples yielded a 6% or less uncertainty. Based on our replicate analyses and those of Farley et al (2001) a 6% uncertainty was assigned to all samples without replicate analyses.

References Cited

Farley, K., Wolf, R., and Silver, L., 1996, The effects of long alpha-stopping distances on (U-Th)/He ages: *Geochimica et Cosmochimica Acta*, v. 60, p. 4223-4229.

Farley, K., Rusmore, M., and Bogue, S., 2001, Post-10 Ma uplift and exhumation of the northern Coast Mountains, British Columbia: *Geology*, v. 29, p. 99–102.

Farley, K.A., 2000, Helium diffusion from apatite: general behavior as illustrated by Durango fluorapatite: *Journal of Geophysical Research*, v. 105, p. 2903-2914.

O'Sullivan, P., and R. Parrish, 1995, The importance of apatite composition and single-grain ages when interpreting fission track data from plutonic rocks: a case study from the Coast Ranges, British Columbia, *Earth and Planetary Science Letters*, 132 (1-4), 213-224.

Table 1: Appendix A. Apatite (U-Th)/He data

Sample	UTM X ^a (m)	UTM Y ^a (m)	Elevation (m asl)	Number of Grains	Number of Replicates	MWAR ^b (μ m)	Mass (μ m)	U (ppm)	Th (ppm)	He (nmol/g)	Ft ^c	Corrected age (Ma)	2 σ Error (Ma)
00MR-14	313348	5669247	1561	multi	1	53.712	24.919	13	24	0.4377	0.78	5.6	0.3
01MR-59	318426	5679729	251	multi	1	63.568	30.723	64	19	0.4905	0.79	1.7	0.1
03TEKI036	312808	5678314	460	single	3	48.569	3.257	14	5	0.1281	0.73	3.0	0.2
00MR-26	321247	5715053	1646	multi	2	34.280	1.038	15	4	0.3750	0.62	7.2	0.4
00MR-15	322453	5676995	1615	multi	1	59.997	28.833	62	11	1.3673	0.79	4.9	0.3
00MR-25	325790	5710954	1695	multi	2	61.420	5.970	9	0	0.1850	0.78	4.8	0.2
00MR-16	327511	5683334	1643	multi	2	54.997	22.876	4	5	0.0488	0.76	2.3	0.1
00MR-18	329953	5685812	1745	multi	4	51.420	4.773	6	7	0.0450	0.77	1.5	0.2
00MR-23	332800	5705565	1695	multi	2	72.850	12.000	9	16	0.2495	0.81	5.6	0.2
00MR-17	335278	5684970	1646	multi	1	77.139	58.748	4	7	0.0918	0.84	3.9	0.2
00MR-22	335368	5700060	1689	multi	1	66.854	44.851	3	1	0.0586	0.82	4.4	0.3
46125	337823	5689319	2260	multi	1	55.200	27.400	4	7	0.0980	0.79	4.4	0.3
00MR-27	339731	5698530	1705	multi	2	65.900	30.500	8	1	0.1532	0.80	3.8	0.2
19148	342432	5694072	4000	multi	1	61.800	40.800	34	16	2.3500	0.81	14.1	0.8
00MR-34	342472	5697610	2830	multi	1	61.711	35.652	12	4	0.4376	0.81	7.5	0.5
00MR-21	342769	5683021	1593	multi	1	61.140	36.900	9	2	0.1727	0.81	4.1	0.3
19154	344576	5698124	2685	multi	1	70.300	79.000	8	2	0.2820	0.83	7.8	0.5
2724R06	344741	5716704	2201	multi	2	66.780	36.820	28	7	1.9230	0.80	15.0	0.8
19151	344786	5695891	3730	multi	1	58.800	35.300	6	2	0.3370	0.80	12.1	0.7
00MR-36	345289	5701419	1362	multi	3	61.950	31.710	45	17	0.9154	0.79	5.3	0.3
00MR-37	348563	5704626	1029	multi	2	72.850	9.150	25	33	0.6760	0.80	5.1	0.3
00MR-20	349859	5679413	1707	multi	1	55.997	30.346	4	3	0.1028	0.79	5.3	0.3
00MR-65	353703	5707424	1628	multi	3	67.610	7.689	12	4	0.4630	0.80	8.6	0.9
00MR-19	354490	5678445	1689	multi	1	60.568	33.045	71	91	3.0262	0.80	7.5	0.5
00MR-38	357233	5704019	750	multi	3	66.370	32.000	26	1	0.6489	0.80	5.4	0.3
56035	357798	5703079	900	multi	1	46.700	36.000	13	2	0.4240	0.77	7.6	0.5

Notes ^a: UTM zone 10, Datum = WGS84; ^b: MWAR is mass-weighted average radius; ^c: Ft is fraction of total alpha particles retained

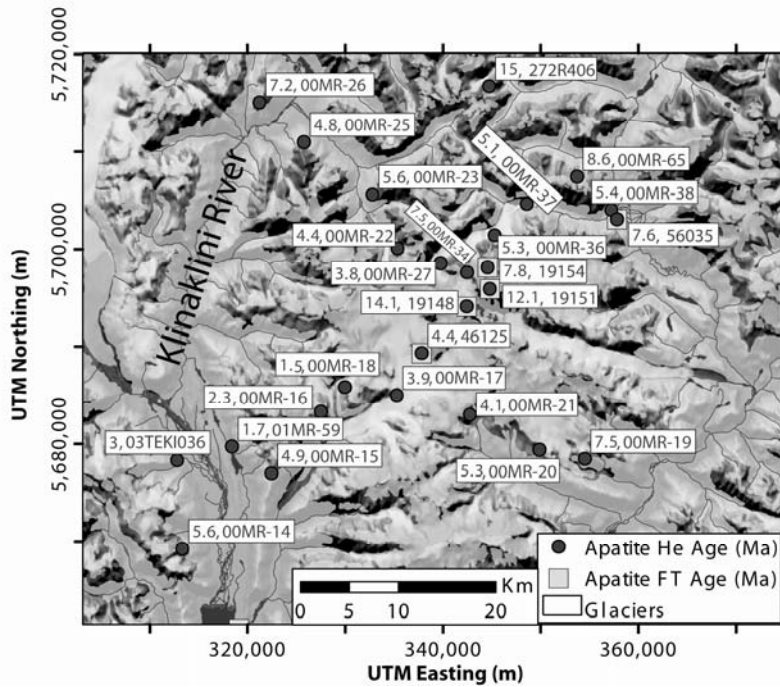


Figure DR1. AHe sample locations, ages, and ID numbers for samples shown in Table 1.

Appendix B: Thermal Model Setup and Assumptions

Numerical thermal and age prediction models: The thermal field of the southern Coast Mountains was simulated using a three-dimensional finite element model modified from Kohl and Hopkirk, (1995) and Kohl, (1999). The model solves the transient advection-diffusion equation using the Galerkin finite-element formulation with an implicit time stepping scheme. An Eulerian reference frame was used for the calculations along with a preconditioned conjugate gradient solver. The model was validated by comparison to analytic solutions of the one-dimensional advection-diffusion equation using both a constant flux and constant temperature lower boundary condition (Carslaw and Jaeger, 1959). Differences between the numerical model and analytic solution were less than 1% for the range of erosion rates considered in this study.

Model predicted apatite (U-Th)/He and apatite fission track ages were calculated by tracking rock cooling histories during the exhumation process. Rock cooling ages were calculated using the kinetic spherical finite element He diffusion and track annealing methods described in Ehlers et al., (2003, 2005). Predicted and observed cooling ages were compared to identify best-fit models using the Chi-squared misfit approach described in Ehlers et al., (2003).

Model geometry, and boundary and initial conditions: Model setup is illustrated in Figure DR2. The model domain has dimensions of 72 x 56 x 35 km in the X, Y, and Z dimensions, respectively. A total of 1.2 million nodes were used with a 250 m spacing in the upper 3 km of the crust. The top surface of the model is a 250 m resolution digital elevation model of the present-day topography. Boundary conditions include a topographic surface constant temperature of 5 C at sea level with an adiabatic atmospheric lapse rate of -7 C/km above sea level. Climate induced variations in surface temperatures likely occur with time but have the greatest effect in the shallow (several hundred meters) subsurface (e.g. Kohl, 1999). The previous surface temperature boundary condition was chosen as our best estimate of the average surface temperature over the simulation durations considered (15 to 20 Ma to present). Side boundary conditions include zero lateral heat flux. A basal flux boundary condition was imposed with variable magnitude between simulations (discussed below). Initial conditions used in each simulation include the steady-state solution of the three-dimensional diffusion equation using the prescribed model geometry and boundary conditions with no erosion. Predicted thermochronometer ages were insensitive to assumed initial condition because of the long duration of simulations (10-20 Myr) relative to the time required (~5 Myr) for the upper crust to reach thermal equilibrium for the simulated erosion rates and initial topography. Material properties were prescribed in the model and not treated as free parameters because of available measurements for thermal conductivity and heat production from neighboring areas of the Coast Plutonic complex (Lewis et al., 1985). Values used for material properties include: thermal conductivity corrected for temperature dependence, $2.7 \text{ Wm}^{-1}\text{k}^{-1}$ (Lewis et al., 1985); density * heat capacity, $2.2 \times 10^6 \text{ Jkg}^{-2}\text{k}^{-1}\text{m}^{-3}$; and heat production, 0.5 uWm^{-3} (Lewis et al., 1985).

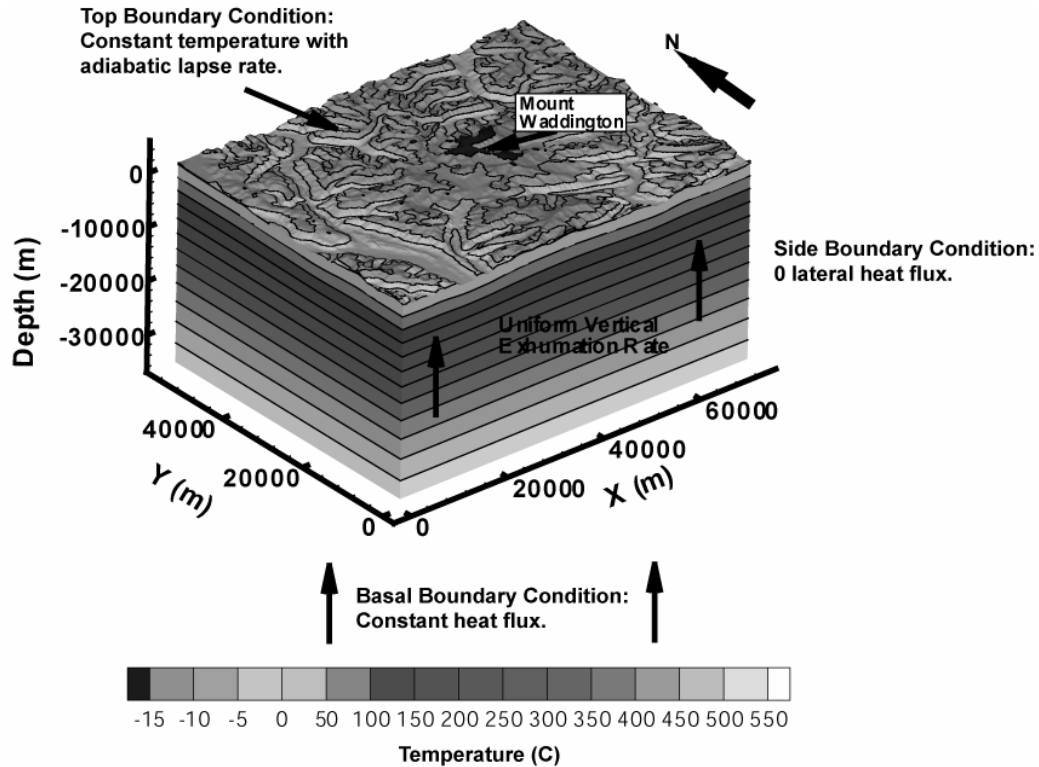
Erosion and topography: A uniform vertical velocity field was used within the model to simulate advective heat transfer by erosional exhumation. The magnitude of erosion rates was variable between simulations (discussed below). Our modeling approach assumes the present day topography was steady-state throughout the simulation. This assumption was made to evaluate the simplest scenario (null hypothesis) of no topographic change throughout the evolution of the orogen. This assumption also allows us to compare model predicted and observed ages on the present day topography to isolate which areas of the orogen have large age anomalies (Fig. 3 of manuscript) and therefore contradict the steady state assumption and suggest transient topography.

Our approach tests the null hypothesis that no significant topographic change has taken place across the orogen since samples passed through closure temperature depths (7 Ma to present). Because we do not explicitly consider the influence of evolving topography on

thermochronometer ages we are not able to reconstruct the exact shape (and relief) of the preglacial topography in this study.

The manuscript highlights the lack of best-fit solutions found for the AHe system and uses the AFT system to constrain the long-term average erosion rate. An assumption of this approach is the lack of sensitivity of the AFT data to paleotopography. Recent work by Ehlers and Farley (2003) shows the relief on the AHe and AFT isotherms beneath the present day topography for an erosion rate of 0.5 mm/yr. Here we test our assumption that AFT data are relatively insensitive to the overlying topography by quantifying how the AFT isotherm structure from Ehlers and Farley (2003), and the measured AFT age, would change if an AFT sample cooled under the paleotopography rather than the present day topography. For example, AFT sample 46125 (Figure 1b) has an age of 11.7 +/- 2.8 Ma (2σ) (O'Sullivan and Parrish, 1995). This sample lies approximately under the paleotopographic high suggested by the AHe data. The relief on the AFT isotherm between this sample location and the present day topographic high is 100 m (Figure 7, Ehlers and Farley, 2003). If the paleotopographic high caused the same deflection of the AFT closure isotherm as the present day topographic high then we can infer our predicted closure temperature depth for sample 46125 could be off by 100 m. Dividing this distance by the model erosion rate (0.5 mm/yr) used to calculate the isotherm position suggests the AFT age for this sample would change by 0.2 Ma if it closed under the paleotopography. This estimated 0.2 Ma error in the predicted AFT age is well within the 2.8 Ma 2σ uncertainty of the sample age. Therefore, we infer that our interpretation of the average long-term erosion rates from the AFT data is not significantly influenced by the use of the present day topography to calculate the subsurface thermal structure of the orogen. In fact, the relief on the AFT isotherm would have to be 1.4 km different than today to produce an AFT age difference that is greater than the sample age uncertainty. This magnitude of change in the AFT isotherm relief would require an unrealistic paleotopographic relief.

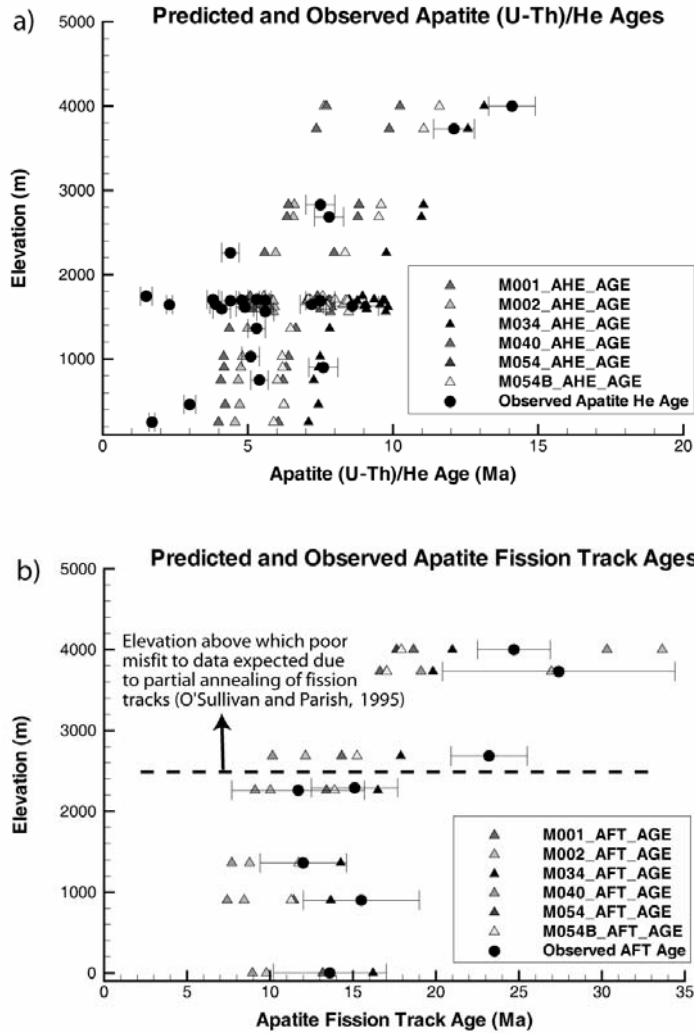
Range of free parameters explored: Free parameters in the model include: (1) basal heat flow, (2) erosional exhumation rate, and (3) erosional exhumation duration. The range of each free parameter simulated in the model includes: basal heat flow of, 10-50 mWm^{-2} (at intervals of 10 mWm^{-2}); erosional exhumation rate, 0.2-1.6 mm yr^{-1} (at intervals of 0.1 mm yr^{-1}); and erosional exhumation duration, 5-20 Myr (at intervals of 2.5 Myr). The product of 5 variations in basal heat flow, 14 variations in exhumation rate, and 7 variations in exhumation duration resulted in a total of 490 thermal simulations used in this analysis to predict thermochronometer ages for the previous range in free parameters. Initial conditions used for each simulation include the steady-state conductive thermal field with no erosion using the prescribed basal heat flow and constant temperature upper boundary condition with an adiabatic atmospheric lapse rate. Thus, 5 different initial conditions were used corresponding to the 5 different basal heat flow values used. The topographic initial condition used for each model is the present-day topography and did not differ between simulations. In each of the 490 simulations conducted the difference (Chi-squared misfit) in predicted and observed thermochronometer ages was used to quantify the fit of the model to the data, and infer how much erosion rates and topography could have changed to produce the observed range of ages.



Appendix Figure DR2. Thermal field and boundary conditions of the numerical model. Result shown is the best-fit model shown in Figure 3a of manuscript. Results shown are for an exhumation rate of 0.38 mm yr^{-1} after 20 Myr of exhumation.

Best-fit Model Results: Figure DR3 shows the measured apatite (U-Th)/He and apatite fission track data (black circles) plotted as a function of sample elevation. The best-fit model predicted ages used for computing age anomalies are also shown (triangles). Figure 1b and 2 in the manuscript show the sample locations on the topography. Both the apatite fission track (O’Sullivan and Parish, 1995) and (U-Th)/He ages increase with sample elevation with a few exceptions of young (U-Th)/He ages collected at a constant elevation of 1600 m (see discussion in manuscript). The model parameters used for the best-fit simulations are shown in Table 2 and the predicted AHe ages used for the age anomalies shown in Figure 3 of the manuscript are presented in Table 3 of appendix B.

The predicted AHe ages for the six best-fit models identified by comparison of model predicted and observed AFT ages (Fig. DR3b). Note that only 5 best-fit models are visible because 2 of the models shown produced identical ages and the symbols plot on top of each other. The AHe age anomalies shown in Figure 3 of the manuscript were computed by taking the difference between the predicted and observed AHe age for samples that have ages less than 7 Ma (the onset time of glaciation of this range). Thus, the inferred acceleration in erosion rates from AHe data occurred sometime over the last 7 Myr.



Appendix Figure DR3: Best fit model predicted, and observed, thermochronometer ages. a) Predicted (triangles) and observed (black circles) apatite (U-Th)/He ages. Data are from Table 1, appendix A. b) Predicted and observed apatite fission track data from O’Sullivan and Parish (1995) used in this study. Model predicted ages shown are from the best-fit models used in this study to reconstruct paleotopography (see discussion in manuscript and Appendix B). Error bars represent 2 sigma uncertainties in sample ages.

Table 2: Appendix B. Best-fit Thermal Model Parameters

Modle Name	Erosion Rate (mm/yr)	Erosion Duration (Ma)	Basal Heat Flow (mWm ⁻²)
M001	0.57	15	20
M002	0.76	10	20
M034	0.4	20	30
M040	0.57	10	40
M054	0.38	20	40
M054b	0.38	17.5	40

Table 3: Appendix B. Best-fit Thermal Model Predicted Ages and Age Anomalies

Sample ID	Observed AHe Age (Ma)	Model M001			Model M002			Model M034		
		Predicted AHe Age (Ma)	AHe Age Anomaly (Ma)	Predicted AFT Age (Ma)	Predicted AHe Age (Ma)	AHe Age Anomaly (Ma)	Predicted AFT Age (Ma)	Predicted AHe Age (Ma)	AHe Age Anomaly (Ma)	Predicted AFT Age (Ma)
00MR-18	1.5	7.4	5.9	12.8	5.6	4.1	9.4	9.0	7.5	15.6
01MR-59	1.7	6.1	4.4	11.2	4.6	2.9	8.2	7.1	5.4	13.3
00MR-16	2.3	7.5	5.2	12.8	5.6	3.3	9.5	9.1	6.8	15.7
03TEKI036	3.0	6.3	3.3	11.4	4.7	1.7	8.4	7.4	4.4	13.6
00MR-27	3.8	7.1	3.3	12.5	5.4	1.6	9.2	8.5	4.7	15.1
00MR-17	3.9	7.2	3.3	12.5	5.4	1.5	9.2	8.7	4.8	15.2
00MR-21	4.1	7.5	3.4	12.9	5.6	1.5	9.5	9.1	5.0	15.7
00MR-22	4.4	7.3	2.9	12.6	5.5	1.1	9.3	8.8	4.4	15.4
46125	4.4	8.0	3.6	13.4	6.0	1.6	10.0	9.8	5.4	16.5
00MR-25	4.8	7.8	3.0	13.0	5.8	1.0	9.6	9.7	4.9	16.1
00MR-15	4.9	7.9	3.0	13.2	5.9	1.0	9.8	9.8	4.9	16.4
00MR-37	5.1	6.4	1.3	11.6	4.8	-0.3	8.6	7.5	2.4	13.8
00MR-36	5.3	6.7	1.4	11.9	5.0	-0.3	8.8	7.8	2.5	14.3
00MR-20	5.3	7.6	2.3	13.0	5.7	0.4	9.6	9.4	4.1	15.9
00MR-38	5.4	6.2	0.8	11.3	4.7	-0.7	8.4	7.3	1.9	13.5
00MR-14	5.6	7.8	2.2	13.2	5.9	0.3	9.8	9.8	4.2	16.3
00MR-23	5.6	7.0	1.4	12.3	5.3	-0.3	9.0	8.5	2.9	14.9

Table 3 (continued): Appendix B. Best-fit Thermal Model Predicted Ages and Age Anomalies

Sample ID	Observed AHe Age (Ma)	Model M040			Model M054			Model M054b		
		Predicted AHe Age (Ma)	AHe Age Anomaly (Ma)	Predicted AFT Age (Ma)	Predicted AHe Age (Ma)	AHe Age Anomaly (Ma)	Predicted AFT Age (Ma)	Predicted AHe Age (Ma)	AHe Age Anomaly (Ma)	Predicted AFT Age (Ma)
00MR-18	1.5	5.1	3.6	8.5	7.6	6.1	13.0	7.6	6.1	13.0
01MR-59	1.7	4.0	2.3	7.2	5.9	4.2	11.0	5.9	4.2	11.0
00MR-16	2.3	5.2	2.9	8.6	7.7	5.4	13.2	7.7	5.4	13.2
03TEKI036	3.0	4.2	1.2	7.5	6.2	3.2	11.3	6.2	3.2	11.3
00MR-27	3.8	4.8	1.0	8.2	7.1	3.3	12.5	7.1	3.3	12.5
00MR-17	3.9	4.9	1.0	8.3	7.3	3.4	12.7	7.3	3.4	12.7
00MR-21	4.1	5.2	1.1	8.6	7.7	3.6	13.2	7.7	3.6	13.2
00MR-22	4.4	5.0	0.6	8.4	7.4	3.0	12.8	7.4	3.0	12.8
46125	4.4	5.6	1.2	9.1	8.4	4.0	13.9	8.4	4.0	13.9
00MR-25	4.8	5.6	0.8	9.0	8.4	3.6	13.7	8.4	3.6	13.7
00MR-15	4.9	5.7	0.8	9.2	8.6	3.7	14.0	8.6	3.7	14.0
00MR-37	5.1	4.2	-0.9	7.5	6.2	1.1	11.4	6.2	1.1	11.4
00MR-36	5.3	4.4	-0.9	7.7	6.5	1.2	11.7	6.5	1.2	11.7
00MR-20	5.3	5.4	0.1	8.8	8.0	2.7	13.5	8.0	2.7	13.5
00MR-38	5.4	4.1	-1.3	7.3	6.0	0.6	11.1	6.0	0.6	11.1
00MR-14	5.6	5.7	0.1	9.2	8.5	2.9	13.9	8.5	2.9	13.9
00MR-23	5.6	4.8	-0.8	8.2	7.2	1.6	12.4	7.2	1.6	12.4

References Cited:

Carslaw, H.S., Jaeger, J.C., 1959, Conduction of heat in solids, Clarendon Press, Oxford, 510 p.

Ehlers, T., and Farley, K., 2003, Apatite (U-Th)/He thermochronometry; methods and applications to problems in tectonic and surface processes: *Earth and Planetary Science Letters*, v. 206, p. 1–14, doi: 10.1016/S0012-821X(02)01069-5

Ehlers, T.A., Willett, S.D., Armstrong, P.A., Chapman, D.S., 2003, Exhumation of the Central Wasatch Mountains: 2 Thermo-kinematic models of exhumation, erosion, and low-temperature thermochronometer interpretation, *Journal of Geophysical Research*, v. 108, 2173, doi:10.1029/2001JB001723.

Ehlers, T.A., Chaudhri, T., Kumar, S., Fuller, C.W., Willett, S.D., Ketcham, R.A., Brandon, M.T., Belton, D.X., Kohn, B.P., Gleadow, A.J.W., Dunai, T.J., Fu, F.Q., 2005, Computational tools for low-temperature thermochronometer interpretation, *Reviews in Mineralogy and Geochemistry*, v. 58, p. 589-622.

Lewis, T.J., Jessop, A.M., Judge, A.S., 1985, Heat flux measurements in southwestern British Columbia: the thermal consequences of plate tectonics, *Canadian Journal of Earth Sciences*, v. 22, p. 1262-1273.

Kohl, T., 1999, Transient thermal effects below complex topographies, *Tectonophysics*, v 306, pp. 311-324.

Kohl, T. and Hopkirk, J., 1995, "FRACTure" a simulation code for forced fluid flow and transport in fractured, porous rock, *Geothermics*, v. 24, pp. 333-343.